An analytical approach for evaluating the impact response of steel fiber reinforced concrete beam

Mohammad Bakhshi [1], Honeyeh Ramezansefat, Mohammadali Rezazadeh, Isabel Valente and Joaquim Barros

[1] Structural Division, Dept. of Civil Engineering, ISISE, Univ. of Minho, 4800-058 Guimarães, Portugal
Mohammad.Bakhshi.ngd@gmail.com

Abstract. In this paper, a new approach is proposed for predicting reaction force in simply supported steel fiber reinforced concrete (SFRC) beams under impact loading (drop weight test) considering the energy conservation approach. If SFRC beams completely fail under impact load, it can be found that the total reaction force is equal to force capacity of SFRC beams. The force-deflection relationship can show the peak force that the SFRC beam can carry under impact load. Since concrete is a material sensitive to loading rates, the strain rate of loading and also the volume fraction of steel fiber will influence the beam´s response. The force-deflection relationship of the SFRC beam under impact loading is obtained using the proposed model. This model considers the effect of volume fraction of steel fiber and also the strain rate on the concrete properties. The model is then verified with the results collected from the literature that include 189 SFRC beams tested under drop-weight impacts and included in a database. The results obtained show that this method can estimate the maximum impact force with acceptable accuracy.

Keywords: Steel fiber reinforced concrete, concrete beam, Drop weight test, Strain rate.

1   Introduction

Steel fiber reinforced concrete (SFRC) is a composite material that includes cement, aggregates, and steel fibers in its composition, [1]. Normal concrete is usually a brittle material, so the addition of fibers causes an increase in its post-cracking tensile capacity and prevents the early cracking of concrete. According to [2-4], SFRC has an improved behavior, which includes: resistance to the combination of wear - tear damage and weathering, high resistance to fatigue stress, excellent impact resistance, excellent tensile strength, ductility, high load capacity after cracking, and high shear strength. The ACI code [1] recognizes the possibility of using a volume content of 0.75% of deformed steel fibers for minimum shear reinforcement in common structural applications under quasi-static loading conditions.

On the other hand, concrete is a material that is sensitive to the strain rate [5-8] imposed during the loading process and, consequently, its mechanical properties are dependent to this rate. The effect of strain rate on concrete for each type of loading is also different (i.e., compressive, tensile, and flexural) [9-12]. Existing experimental results on the dynamic behavior of SFRC have shown that both the tensile strength and the mode I fracture energy increase with strain rate, [2,3]. Moreover, based on the experimental results, the strain rate influences on the reaction force and energy dissipation capacity of SFRC beam. The dynamic increase factor (DIF) of compressive, tensile and flexural strength of SFRC are defined to evaluate the effect of strain rate on the SFRC characterizations [6-9]. Although there are some experimental studies for understanding the flexural behavior of SFRC under impact load [5-12], due to include several aspects, analytical models for predicting the impact response of SFRC beams are still scarce. To accurately predict the impact response of SFRC beams under the drop-weight impact, some analytical methods for concrete beams reinforced with conventional steel bars (RC beams) can be adapted for SFRC beams. There are generally three approaches for predicting the impact response of a RC beam, namely, contact law, energy-based approach, and spring-mass model [13]. These approaches are used in RC beams because complete fracture of this beams does not occur. In SFRC beams under impact load, the total energy applied by the impactor is dissipated by the inertial energy caused by existing acceleration and deflection of the beam. If SFRC beams completely fail under impact load, it can be found that the total reaction force is equal to force capacity of SFRC beams. In this condition, the impactor passes the beam and the remaining energy of the impactor is released to the test setup frame. Consequently, for each SFRC beam, critical initial kinetic energy can be defined as the maximum initial kinetic energy that the beam can dissipate. A simplified method is established in this paper for predicting the maximum reaction force of simply supported SFRC beams under impact load (Fig. 1). Appropriate assumptions and theoretical derivation are utilized to establish this simplified method. Moreover, the results of 189 SFRC beams under impact load acting at midspan are compiled in a database to validate the proposed method.

2   Analytical method

In the impact loading condition, due to the existing accelerations on the beam, the inertia force is mobilized along the beam, and its direction is contrary to the direction of the beam's movement. The total impact force (P_t) in a simply supported beam is equal to the sum of the total inertia forces (P_i) and reaction forces R_1 and R_2 in its supports ($P_b = R_1 + R_2$), (Fig. 1). By assuming the linear acceleration distribution, the inertia force is calculated by the Eq. (2) [4].

$$P_t = P_b + P_i \tag{1}$$

$$P_i = \rho A \ddot{\delta}(t) \left[\frac{l}{3} + \frac{8}{3} \frac{s^3}{l^2} \right] \tag{2}$$

where ρ, A, l, s and $\ddot{\delta}(t)$ are the beam's material density, cross section area, span length, overhanging length (Fig. 2), and the time dependent acceleration of beam at its midspan, respectively.
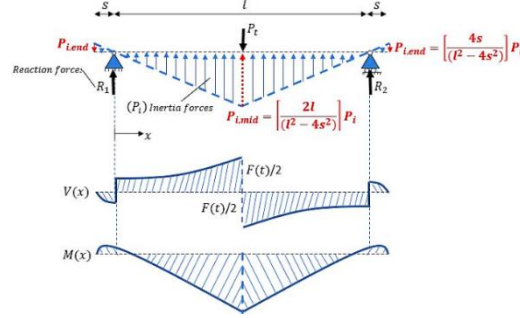

Fig. 1. Loadings and generated shear and bending moment diagrams in an impact situation.

The acceleration is depended on the materials properties, geometry of the beam, and the height and mass of impactor. Unfortunately, there are not enough data about the maximum acceleration in the midspan of the beam. The statistical analysis of the available experimental studies [6, 8, 11, 22] shows that the effects of the stiffness of the beam and mass of impactor have a marginal impact on the maximum acceleration, while by increasing the height of the impactor, the acceleration increases significantly. Considering the lack of experimental investigations, a simple empirical equation is proposed by using the available experimental data for calculating the maximum acceleration at midspan ($\ddot{\delta}_{max}$) based on the height of the impactor (H) as follows:

$$\ddot{\delta}_{max} = \left(-6.404\times10^3\right)H^3 + \left(1.776\times10^4\right)H^2 - \left(3.665\times10^3\right)H + 4980 \qquad (3)$$

In the current study, first, the force-deflection relation of SFRC simply supported beam is analytically predicted using the proposed model, whose governing variables are function of the strain rate of loading, and then a simplified approach is proposed to determine its loading capacity.

2.1 Force-deflection relationship of SFRC

Several studies in the literature focused on the stress-strain relation of SFRC materials. The model proposed by Barros *et al.* [18] was selected in the present research because it considers the effect of steel fiber volume as the main parameter (Table.1). Since concrete is a sensitive material to the strain rate of loading, its static constitutive quantities must be updated when exposed to loading conditions that generate high strain rates. In the current study, for considering the effect of the strain rate on the compressive strength and modulus of elasticity, *fib*-Model code 2010 formulation is adopted, by considering Eqs. (4) and (5) [17]. On the other hand, since the effect of fiber reinforcement mostly influence the tensile behavior of concrete, rather than the compressive behavior, to consider the strain rate effect on the tensile strength of SFRC, the model

4

proposed by Malver and Ross is adopted (Eq. (6)) [19], because their proposed model is supported on results from experimental tests with SFRC specimens.

$$\frac{f'_{cd}}{f'_{cs}} = \begin{cases} \left(\dfrac{\dot{\varepsilon}_c}{30\times10^{-6}}\right)^{0.014}, & \dot{\varepsilon}_c \leq 30 \ s^{-1} \\[3mm] 0.012\left(\dfrac{\dot{\varepsilon}_c}{30\times10^{-6}}\right)^{\frac{1}{3}}, & \dot{\varepsilon}_c > 30 \ s^{-1} \end{cases} \tag{4}$$

$$\frac{E_{cd}}{E_{cs}} = \left(\frac{\dot{\varepsilon}_c}{30\times10^{-6}}\right)^{0.026} \tag{5}$$

$$\frac{f'_{td}}{f'_{ts}} = \begin{cases} \left(\dfrac{\dot{\varepsilon}_t}{1\times10^{-6}}\right)^{\delta}, & \dot{\varepsilon}_c \leq 1 \ s^{-1} \\[3mm] \beta\left(\dfrac{\dot{\varepsilon}_t}{1\times10^{-6}}\right)^{\frac{1}{3}}, & \dot{\varepsilon}_c > 1 \ s^{-1} \end{cases}, \quad log(\beta) = 6\delta - 2, \quad \delta = 1/(1+0.6f'_c) \tag{6}$$

Table 1. Stress-strain model of SFRC suggested by Barros [18].

Compressive	Tensile
$\dfrac{\sigma_{cf}}{f'_{cf}} = \dfrac{\left(\dfrac{\varepsilon_c}{\varepsilon'_{cf}}\right)}{(1-p-q)+q\left(\dfrac{\varepsilon_c}{\varepsilon'_{cf}}\right)+p\left(\dfrac{\varepsilon_c}{\varepsilon'_{cf}}\right)^{(1-q)/p}}$ $p+q = 1-\dfrac{f'_{cf}}{E_c\varepsilon'_c}$ $\varepsilon'_{cf} = 2.2\times10^{-3} + 0.0002W_f$ $p = 1 - 0.919\exp(-0.394W_f)$ $W_f \simeq 3V_f$	$\sigma = \begin{cases} E_{ci}\varepsilon, & \varepsilon \leq \varepsilon_{cr} \\ E_{ci}\left(\dfrac{\alpha-1}{p_1-1}\right)(\varepsilon-\varepsilon_{cr})+f_{ct}, & \varepsilon_{cr} < \varepsilon \leq p_1\varepsilon_{cr} \\ E_{ci}\left(\dfrac{\alpha}{p_1-p_2}\right)(\varepsilon-p_2\varepsilon_{cr}), & p_1\varepsilon_{cr} < \varepsilon \leq p_2\varepsilon_{cr} \end{cases}$ $E_{ci} = \left(\dfrac{f_{ct}}{\varepsilon_{cr}}\right), \quad \varepsilon_{cr} = \dfrac{f_{ct}}{E_{ci}}, \quad f_{ct} = 1.4\left(\dfrac{f'_c-8}{10}\right)^{\frac{2}{3}}$ $E_{ci} = 2.15\times10^4\left[\dfrac{f'_c}{10}\right]^{\frac{1}{3}}, \quad \alpha = \dfrac{L(beam\ length)}{l(span\ length)}-1, \quad \dfrac{G_f}{G_{f0}} = 19.953 + 3.213W_f$ $G_{f0}(N.mm^{-1}) = f(max.agg.size\ and\ f'_c), \quad G_{f0} = \begin{cases} 0.025, & d = 8mm \\ 0.030, & d = 16mm \\ 0.058, & d = 32mm \end{cases}$ $l_b = \dfrac{G_f E_{ci}}{f_{ct}^2} = 10970\ G_{f0}\dfrac{\left(\dfrac{f'_c}{10}\right)^{1.03}}{\left[\left(\dfrac{f'_c}{10}\right)-0.8\right]^{\frac{1}{3}}}, \quad p_2 = \dfrac{2G_f}{\alpha l_b f_{ct}\varepsilon_{cr}} - \dfrac{p_1-\alpha}{\alpha}, \quad p_1 = 1\sim3 \simeq 2$

In Eqs. (4) to (6), f'_{cd} and f'_{cs} are, respectively, the dynamic and static compressive strength, f'_{td} and f'_{ts} are, respectively, the dynamic and static tensile strength, E_{cd} and E_{cs} are, respectively, the dynamic and static modulus of elasticity, while $\dot{\varepsilon}_c$ and $\dot{\varepsilon}_t$ are, respectively, the compressive and tensile strain rate. Since the concrete compressive strength is about ten times higher its tensile strength, the overall behavior of the SFRC beam is often controlled by the tensile behavior. In this regard, the tensile strength, fracture energy, and modulus of elasticity of the SFRC are essential parameters for calculating the overall behavior of the beam under impact load. According to the experimental results [9-12], the post peak tensile behavior of SFRC under impact load can be considered linear concerning the effect of strain rate on the fracture energy. Based on the experimental stress-strain curves of the SFRC under various strain rates, the value of fracture energy under static and dynamic loading can be calculated by Eq. (7)

[12, 23]. The first term of the equation represents the fracture energy externally supplied to propagate the crack across the specimen. The second term of Eq. (7) corresponds to the fracture energy supplied by the beam weight, causing to reduce the prediction error compared to the recommendation of RILEM TC50-FMC Technical Committee [24] which did not consider the influence of the cantilever of the beam:

$$G_f = \frac{W_0}{b(h-a)} + \frac{mg\left(1 - \frac{l}{2s}\right)\delta_u}{b(h-a)} \qquad (7)$$

where W_0, b, h, a, s, l, m, δ_u, and g are the area under the experimental load-displacement curve, width, cross section's height, notch depth, span, length, mass of the beam between the supports (length l), final deflection of the beam and gravitational acceleration, respectively. For the case of impact loading, due to the existing inertia force, W_0 is the area under the reaction force-displacement curve [23]. To consider the effect of the strain rate of loading on the fracture energy of SFRC, the model proposed by Zhang *et al.* [12] for determining the DIF of fracture energy is adopted as follows:

$$DIF_G = \frac{G_{fd}}{G_{fs}} = 1 + (7.6 \times 10^{-6}) \left(\frac{\dot{\delta}_d}{\dot{\delta}_s}\right)^{1.54}; \qquad \dot{\delta}_s = 1 \left(mm/s\right) \qquad (8)$$

where G_{fd} and G_{fs} are fracture energy of the SFRC beam under dynamic and static loading, respectively, which can be calculated by Eq. (7). $\dot{\delta}_d$ and $\dot{\delta}_s$ (=1 mm/s) are the dynamic and static loading rate in mm/s, respectively. On the other hand, according to three-point bending test, the strain rate ($\dot{\varepsilon}$) can be obtained based on the beam bending theory by using the displacement rate ($\dot{\delta}$) as follows [22]:

$$\dot{\varepsilon} = \frac{6h\dot{\delta}}{L^2} \qquad (9)$$

where h and l are the cross section's height and span length of the beam, respectively. After determining the fracture energy parameter, to define the post cracking tensile behavior, the softening constitutive relationship must be derived from the fracture parameters, namely, the tensile strength, the width of the fracture process zone (l_b), the mode I fracture energy (G_f), and the shape of the softening diagram. The area under the post-cracking tensile stress-strain curve (g_f) can be defined from the following equation, proposed by Barros *et al.* [18]:

$$g_f = \frac{G_f}{l_b} \qquad (10)$$

where l_b can be taken as approximately three times the maximum aggregate size, as proposed by Bazant and Oh [20], for plain concrete, [18]. By ignoring the effect of strain rate on l_b, the DIF of the area under the tensile stress-strain curve was assumed to be the same as DIF of the fracture energy (Fig. 3).

$$DIF_G = DIF_{g_f} = \frac{A_d}{A_s} = \frac{0.5 f'_{td} \times (\xi - 1) \varepsilon_{cr,d}}{\left[0.5 f'_{ts} \varepsilon_{cr} (\alpha + 1)(p_1 - 1) \right] + \left[0.5 f'_{ts} \varepsilon_{cr} \times \alpha (p_2 - p_1) \right]} \qquad (11)$$

where A_d and A_s are the area under the dynamic and static post-cracking tensile stress-strain curve, respectively (Fig. (3)). In Eq. (11) ε_{cr} and $\varepsilon_{cr,d}$ are the strain at concrete crack initiation in static and dynamic loading conditions, respectively, α, p_1 and p_2 are coefficients defining the bilinear configuration of the constitutive law. For defining the tensile behavior of SFRC under impact load, it should be considered that the fracture mechanism of steel fibers in SFRC composite material is different in the various rate of loading. For example, for hooked end fibers, by increasing the rate of loading the mechanism of steel fibers changes from pull-out to rupture resulting in post-cracking the slope of the tensile stress-strain curve SFRC increases. In high strain rate loading, hooked end steel fibers mostly fail by tensile rupture, while under static loading the fibers are pulled out, enhancing the maximum deflection of SFRC under tensile and bending tests. In this regard, the tensile stress-strain curve of SFRC under impact load can be simplified by two linear branches, as shown Fig. 3. The linear behavior up to the peak point can be defined by Eqs. (5) and (6), and the post-peak behavior, can be obtained by Eqs. (8) to (11) considering the effect of strain rate on fracture energy of SFRC. By adopting the model proposed by Barros *et al.* [18] for the tensile behavior of SFRC under static loading and the model suggested by Malver and Ross [19] for the effect of strain rate on the tensile strength of SFRC materials, ξ can be calculated by Eqs. (8) to (11).
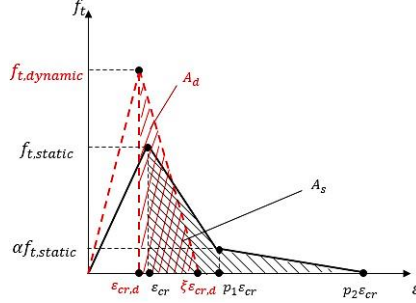

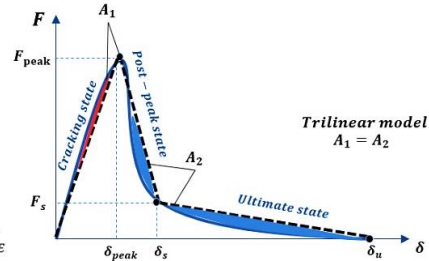**Fig. 2.** Dynamic tensile behavior of the SFRC. **Fig. 3.** Moment-curvature relationship.

In general, the nonlinear analysis of beams can be conducted with the moment-curvature relationship based on the layered-section approach. In the present study, to determine the moment-curvature relationship of a cross-section, the sectional analysis software DOCROS has been used [21]. The compressive and tensile stress-strain relations of SFRC have been modified for dynamic loading, and they are utilized as a material model in DOCROS. Fig. 3 presents a schematic representation of the moment-curvature relationship of a SFRC beam's section, including the cracking, post-peak, and ultimate state. The moment-curvature diagram can be simplified to a trilinear curve that the area under the moment-curvature curve remains constant. For achieving the force-deflection diagram of the SFRC beam under impact load, the moment distribution on the beam

must be calculated considering the effect of inertia force. Because the inertia force along the beam changes the moment distribution. The moment distribution can be obtained using the ratio of inertia force to total force (Fig. 2). The ratio of inertia force to total force (β) was defined because analyzing the beam under impact load is completely different from analyzing the beam under static load. In the Eq. (12), the inertia force (P_i) is obtained by Eq. (1) and β is a function of P_b . Thus, P_b could be achieved through a try and error process. $M(x)$ is the moment distribution along the beam and is the total force that in

$$\beta = \frac{P_i}{P_t} = \frac{P_i}{P_i + P_b}; \qquad M(x) = \left(\frac{2}{3}\beta\right)\left(\frac{F}{l^2}\right)x^3 + \left(\frac{1-\beta}{2}\right).F.x \qquad (12)$$

where F is the total force that is increasing smoothly from zero up to peak value and then decreases up to zero at the ultimate deflection. By considering the peak moment (M_{peak}), the peak force (F_{peak}) in the midspan ($x = l/2$) can be obtained. The post-peak force (F_s) can be obtained by the same approach considering the M_s instead of M_{peak} . Using the conjugate beam method, the curvature can be considered as a load (Fig. 5). In this condition, the moment of every point of the conjugate beam is equal to the deflection of the main beam. There are three necessary points to draw the force-deflection diagram; (a) peak point (δ_{peak} , F_{peak}); (b) post-peak point (δ_s , F_s); and (c) ultimate point (δ_u ,0). As was mentioned, the force values of these three points can be calculated by Eq. (12). The peak deflection (δ_{peak}) can be achieved by Eq. (15). For calculating the post-peak deflection (δ_s) and ultimate deflection (δ_u) firstly two hypothetical moments (M_s' and M_u') are defined. These moments are equivalent curvatures ϕ_s and ϕ_u in linear and rigid behavior of the beam (Fig. 6). Two equivalent forces (F_s' and F_u') can be defined by Eq. (12) based on the moment of M_s' and M_u' . Accordingly, the post-peak deflection (δ_s) and ultimate deflection (δ_u) are calculated by using the Eq. (16).

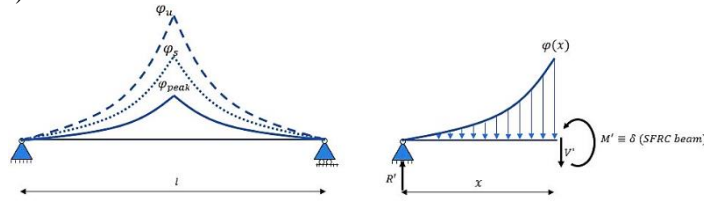**Fig. 4.** Conjugate beam method.

$$\phi(x) = M(x).\left(\frac{\phi_{peak}}{M_{peak}}\right) \qquad (13)$$

$$R' = \frac{1}{2}\int_0^l M(x).\left(\frac{\phi_{peak}}{M_{peak}}\right)dx = \left(Fl^2\right)\left(\frac{3-\beta}{24}\right)\left(\frac{\phi_{peak}}{M_{peak}}\right) \qquad (14)$$

$$\delta_{peak} = \frac{(10-\beta)}{240} \times l \times \frac{\phi_{peak}}{M_{peak}} \times F_{peak} \; l^2 \qquad (15)$$

$$\delta_s = \frac{(10-\beta)}{240} \times l \times \frac{\phi_{peak}}{M_{peak}} \times F_s' \, l^2; \quad and \quad \delta_u = \frac{(10-\beta)}{240} \times l \times \frac{\phi_{peak}}{M_{peak}} \times F_u' \, l^2 \qquad (16)$$

In Eq. (13), $\phi(x)$ is the distribution curvature along the beam. Finally, based on the previously calculated moment-curvature diagram, the force-deflection diagram of the beam under dynamic loading is finalized, as shown in Fig. 7.
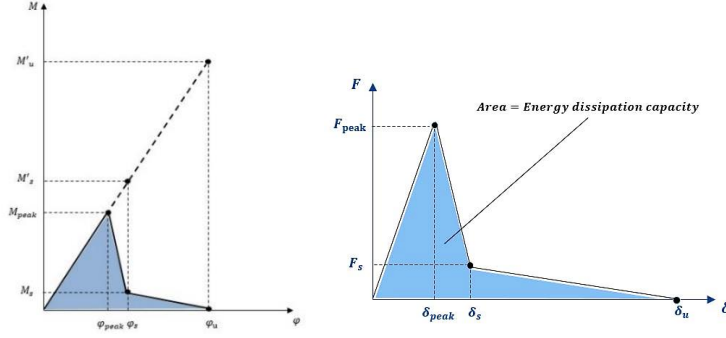

Fig. 5. Defining the assumed moments, F_s' and F_u' .   **Fig. 6.** Force-deflection diagram of SFRC.

The following equation provides the area under the $F - \delta$ diagram, which represents the energy dissipation capacity of the SFRC beam under impact loading.

$$\int_0^{\delta_u} F(\delta)d\delta = \left[\frac{F_{peak} \cdot \delta_{peak}}{2}\right] + \left[\frac{\left(F_{peak} + F_s\right)\left(\delta_s - \delta_{peak}\right)}{2}\right] + \left[\frac{F_s \cdot \left(\delta_u - \delta_s\right)}{2}\right] \qquad (17)$$

where F_{peak} , δ_{peak} , F_s , δ_s , and δ_u are the peak force, deflection at peak force, post-peak force, deflection at post-peak force, and ultimate deflection, respectively.

2.2   Maximum reaction force

The energy balance equation can be written for the SFRC beam under the dropping down of the impactor. It should be noted that the complete fracture may happen in the SFRC beam under impact loading. In this condition, extra kinetic energy of impactor after passing the beam releases to the test setup frame. Consequently, for each SFRC beam, critical initial kinetic energy ($E_{k,cr}$) can be defined as the maximum initial kinetic energy that the beam can dissipate. In other words, the critical initial kinetic energy is the minimum energy to fracture the SFRC beam completely. The critical initial kinetic energy can be calculated using the energy balance equation:

$$E_{k,cr} + U = E_{cap.} \qquad (18)$$

$$E_{k,cr} = E_{cap.} - U = \int_0^{\delta_u} F(\delta)d\delta - (m+m')g\delta_u \qquad (19)$$

where U is the potential energy of the beam caused by deflection (Fig. 8), and $E_{cap.}$ is the energy dissipation capacity of the beam. In Eq. (19) g, m' and m are the gravity acceleration, the mass of impactor and the mass of the beam, respectively (Fig. 8). The energy balance equation, can be written for each value of initial kinetic energy:

$$E_{k,1} + U = E_c \quad \rightarrow \quad \frac{1}{2}m'V_1^2 + (m+m')g\delta_{max} = \int_0^{\delta_{max}} F(\delta)d\delta; \qquad E_{k,1} \le E_{k,cr} \tag{20}$$

$$E_{k,1} + U = E_{cap.} + E_{k,2} \quad \rightarrow \quad \frac{1}{2}m'V_1^2 + (m+m')g\delta_u = \int_0^{\delta_u} F(\delta)d\delta + \frac{1}{2}m'V_2^2; \qquad E_{k,1} > E_{k,cr} \tag{21}$$

where $E_{k,1}$ is the initial kinetic energy that impactor applies to the beam at V_1 initial velocity, $V_1 = \sqrt{2gH}$ (H is the distance of the impactor to the beam's surface of impact). If the beam after impact loading does not fail, the initial energy is completely dissipated by the beam, being applicable Eq. (20). However, if the beam fails and separates into two segments, the difference between the initial kinetic energy and the energy dissipation capacity of the beam releases to test set up frame. In this case, the extra energy is considered as the second kinetic energy. In this condition, the velocity of the impactor is V_2. Consequently, there are generally two conditions: (a) the initial kinetic energy is more than the critical kinetic energy ($P_b = F_{peak} - P_i$) and (b) the initial kinetic energy is less than the critical kinetic energy, Eq. (22). If the initial kinetic energy is less than the critical kinetic energy, the maximum total force depends on the maximum deflection that can be obtained by Eqs. (20) and (21). Clearly, due to the softening behavior of SFRC composite after the peak force, after the peak deflection, the maximum force that the beam has experienced is equal to the peak force (Fig. 9). Thus, the maximum force can be calculated by Eq. (22).

$$P_b = \begin{cases} F(\delta_{max}) - P_i, & \delta_{max} < \delta_{peak} \\ F_{peak} - P_i, & \delta_{max} \ge \delta_{peak} \end{cases} \tag{22}$$
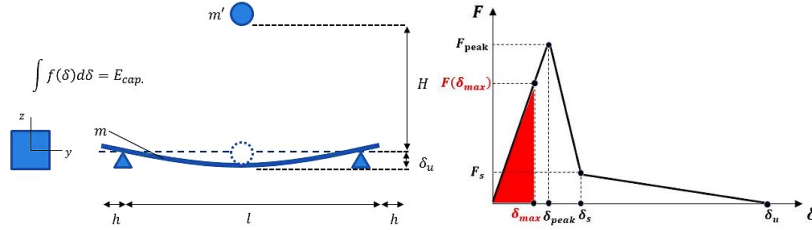

Fig. 7. Schematic shape of the beam under impact load. **Fig. 8.** The maximum response of beam.

3 Assessment of the proposed method

To validate the proposed method for predicting the peak response of SFRC beams under impact loading, a database of 189 SFRC beams tested under drop-weight impact at

midspan is collected from other studies in the literature [6-12]. All the specimens considered in this study are simply supported SFRC beams with rectangular cross-section, and the impactors have two types of nose shape: spherical and flat impact surface.

Method C (considering the proposed model for tensile post-peak behavior (Fig. 3) and the model proposed by Malver and Ross [19] for calculating the effect of strain rate on the tensile strength) was selected to determine the force-deflections curve of SFRC beam under impact loading. For understanding the effect of DIF formulation on the force-deflection diagram, the Method B (considering the proposed model for tensile post-peak behavior (Fig. 3) and the model proposed by *fib* Model Code [17] for calculating the effect of strain rate on the tensile strength) was selected. Moreover, for evaluating the effect of the tensile post-peak behavior of SFRC on the force-deflection curve, Method A (using the equation of Barros *et al.* [18] for post-peak behavior (Table 1) and the model proposed by Malver and Ross [19] for calculating the effect of strain rate on the tensile strength) was also performed. Thus, three methodologies were selected to evaluate the force-deflection diagrams (Fig. 10 and 11).
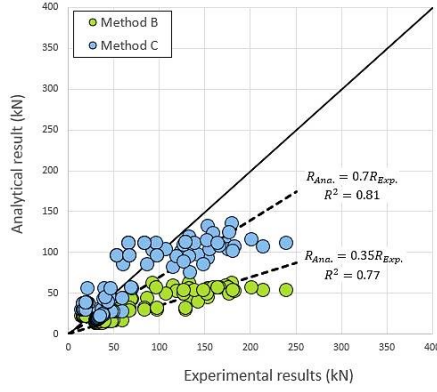

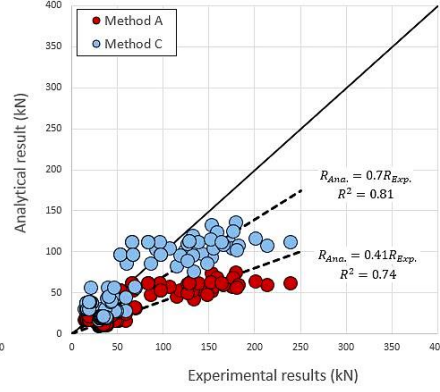**Fig. 9.** Comparison of the methods C and B.   **Fig. 10.** Comparison of the methods C and A.

Generally, the analytical results of all methods underestimated the experimental results. However, by considering the suggested approach (Method C) for predicting the maximum impact force of the SFRC beam on the simple supports, the tensile behavior of SFRC is updated based on different strain rates (Eqs. (6) and (11)). In this condition, the results have shown much higher accuracy than the Methods A and B (Fig. 10 and 11). As can be seen in the present paper, based on the proposed approach, the minimum energy for the failure of the SFRC beam can be estimated by the properties and the geometry of material, Eqs. (20) and (21). There are several methods for evaluating the accuracy of the model to predict the reaction force of the SFRC beam under impact loading. In the present study, the mean absolute deviation (MAD) and mean absolute percentage error (MAPE) have been used.

$$MAD = \frac{\sum_{1}^{N} |pre_i - exp_i|}{N}, \quad and \quad MAPE = \frac{1}{N}\sum_{1}^{N} \left|\frac{pre_i - exp_i}{exp_i}\right| \times 100 \qquad (23)$$

where *pre* is the model predictions, *exp* is the experimental results, and N is the total number of specimens. The value of MAD and MAPE for the proposed model (Method C) are 23. 52 and 41.69 respectively while for the Method A are 40.99 and 52.82 and for Method B are 38.18 and 50.44 respectively. Obviously, by increasing the number of data, the precision of the model may be enhanced. It can be seen that method C can predict the results more precisely.

4   Conclusion

In the current study, the impact response of steel fiber reinforced concrete (SFRC) beams has been analytically investigated and a new approach for predicting reaction force of simply supported SFRC beams under impact loading (drop weight test) has been proposed. Based on the work carried out, the conclusions are:

(1) The proposed method consider the effect of strain rate on the tensile strength and also the post-peak behavior of SFRC. Moreover, this model can be used for a wide range of impact weight and velocity, geometry of beam, and volume fraction of steel fiber.
(2) A comparison with 189 experimental tests has shown that the proposed method is able to estimate the reaction forces of SFRC beams under impact loading. The reaction force is shown to be slightly underestimated.
(3) Based on the existed experimental tests, the results have shown the proposed method can predict the experimental results more precisely and realistic than the other method that consider the static function for the impact loading.

Acknowledgments

References

1. American Concrete Institute, ACI 318-11: Building Code Requirements for Structural Concrete and Commentary, American Concrete Institute, Framington Hills, MI, 2011.
2. Thomas, R. J., & Sorensen, A. D. (2017). Review of strain rate effects for UHPC in tension. Construction and Building Materials, 153, 846-856.
3. Fujikake, K., Senga, T., Ueda, N., Ohno, T., & Katagiri, M. (2006). Effects of strain rate on tensile behavior of reactive powder concrete. Journal of Advanced Concrete Technology, 4(1), 79-84.

4. Banthia, N., Chokri, K., Ohama, Y., & Mindess, S. (1994). Fiber-reinforced cement based composites under tensile impact. Advanced Cement Based Materials, 1(3), 131-141.
5. Wang, N., Mindess, S., & Ko, K. (1996). Fibre reinforced concrete beams under impact loading. Cement and concrete research, 26(3), 363-376.
6. Ulzurrun, G., & Zanuy, C. (2017). Flexural response of SFRC under impact loading. Construction and Building Materials, 134, 397-411.
7. Millard, S. G., Molyneaux, T. C. K., Barnett, S. J., & Gao, X. (2010). Dynamic enhancement of blast-resistant ultra-high performance fibre-reinforced concrete under flexural and shear loading. International Journal of Impact Engineering, 37(4), 405-413.
8. Zanuy, C., & Ulzurrún, G. S. (2017). Rate effects of fiber-reinforced concrete specimens in impact regime. Procedia engineering, 193, 501-508.
9. Hao, Y., Hao, H., & Chen, G. (2016). Experimental investigation of the behaviour of spiral steel fibre reinforced concrete beams subjected to drop-weight impact loads. Materials and Structures, 49(1-2), 353-370.
10. Yoo, D. Y., Yoon, Y. S., & Banthia, N. (2015). Flexural response of steel-fiber-reinforced concrete beams: Effects of strength, fiber content, and strain-rate. Cement and Concrete Composites, 64, 84-92.
11. Banthia, N., Gupta, P., & Yan, C. (1999). Impact resistance of fiber reinforced wet-mix shotcrete part 1: Beam tests. Materials and Structures, 32(8), 563.
12. Zhang, X. X., Elazim, A. A., Ruiz, G., & Yu, R. C. (2014). Fracture behaviour of steel fibre-reinforced concrete at a wide range of loading rates. International Journal of Impact Engineering, 71, 89-96.
13. Pham, T. M., & Hao, H. (2016). Prediction of the impact force on reinforced concrete beams from a drop weight. Advances in Structural Engineering, 19(11), 1710-1722.
14. Hazizan, M. A., & Cantwell, W. J. (2003). The low velocity impact response of an aluminium honeycomb sandwich structure. Composites Part B: Engineering, 34(8), 679-687.
15. Lu, G., & Yu, T. X. (2003). Energy absorption of structures and materials. Elsevier.
16. Wu, M., Chen, Z., & Zhang, C. (2015). Determining the impact behavior of concrete beams through experimental testing and meso-scale simulation: I. Drop-weight tests. Engineering Fracture Mechanics, 135, 94-112.
17. Model Code 2010-Final draft: Volume 1. Vol. 65. fib Fédération internationale du béton, 2012.
18. Barros, J. A., & Figueiras, J. A. (1999). Flexural behavior of SFRC: testing and modeling. Journal of materials in civil engineering, 11(4), 331-339.
19. Malvar, L. J., & Ross, C. A. (1998). Review of strain rate effects for concrete in tension. ACI Materials Journal, 95, 735-739.
20. Bažant, Z. P., & Oh, B. H. (1983). Crack band theory for fracture of concrete. *Matériaux et construction*, 16(3), 155-177.
21. Ramezansefat, H., Barros, J., & Rezazadeh, M. (2017). A model for the simultaneous prediction of the flexural and shear deflections of statically determinate and indeterminate reinforced concrete structures. *Structural Concrete*, 18(4), 618-633.
22. Othman, H., Marzouk, H., & Sherif, M. (2019). Effects of variations in compressive strength and fibre content on dynamic properties of ultra-high performance fibre-reinforced concrete. Construction and Building Materials, 195, 547-556.
23. Zhang, X., Ruiz, G., Tarifa, M., Cendón, D., Gálvez, F., & Alhazmi, W. (2017). Dynamic Fracture Behavior of Steel Fiber Reinforced Self-Compacting Concretes (SFRSCCs). *Materials*, 10(11), 1270.
24. RILEM TC 50-FMC Determination of the fracture energy of mortar and concrete by means of three-point bend tests on notched beams. Mater. Struct. 1985, 18, 99–101